New Journal of Physics
The open access journal at the forefront of physics
Deutsche Physikalische Gesellschaft DPG | IOP Institute of Physics

Magneto-optical Kerr effect in resonant subwavelength nanowire gratings

H Marinchio[1], R Carminati[1], A García-Martín[2] and J J Sáenz[3,4,5]

[1] Institut Langevin, ESPCI ParisTech, CNRS, 1 rue Jussieu, F-75238 Paris Cedex 05, France
[2] IMM-Instituto de Microelectrónica de Madrid (CNM-CSIC), Isaac Newton 8, PTM, E-28760 Tres Cantos, Madrid, Spain
[3] Condensed Matter Physics Center (IFIMAC), Departamento de Física de la Materia Condensada and Instituto 'Nicolás Cabrera', Universidad Autónoma de Madrid, E-28049 Madrid, Spain
[4] Donostia International Physics Center (DIPC), Paseo Manuel Lardizabal 4, E-20018 Donostia-San Sebastian, Spain
E-mail: juanjo.saenz@uam.es

Received 29 June 2013, revised 14 November 2013
Accepted for publication 21 November 2013
Published 9 January 2014

New Journal of Physics **16** (2014) 015007

doi:10.1088/1367-2630/16/1/015007

Abstract

Periodic arrays of nanorods can present a resonant response at specific geometric conditions. We use a multiple scattering approach to analyze the optical response of subwavelength nanowire gratings made of arbitrary anisotropic materials. When the rods are made of magneto-optical dielectrics we show that there is a complex interplay between the geometric resonances of the grating and the magneto-optical Kerr effects (MOKE) response. As we will show, for a given polarization of the incident light, a resonant magneto-optical response can be obtained by tuning the incidence angle and grating parameters to operate near the resonance condition for the opposite polarization. Our results could be important to understand and optimize MOKE structures and devices based on resonant subwavelength gratings and could open new perspectives in sensing applications.

[5] Author to whom any correspondence should be addressed.

1. Introduction

Periodic structures and the propagation of light through them has been an interesting topic for more than a century. Even before the boost in activity with the development of the photonic crystals Wood [1], in 1902, reported the existence of singularities (known as Wood's anomalies) in the reflectance of one-dimensional (1D) metallic gratings. In fact, there were two different types of anomalies identified by Fano [2]. One can be identified as discontinuous changes of intensity along the spectrum at given frequencies [3]. The other is due to a resonance effect [4] that takes place when the external wave couples with quasi-stationary waves confined in the grating. After the observation of enhanced transmission through a two-dimensional (2D) array of subwavelength holes drilled in an otherwise opaque metallic film [5], there was a renewed interest in studying the physics of both reflection and transmission 'anomalies'. The enhanced transmission in noble metals is commonly associated with the excitation of surface plasmons, but other type of diffraction resonances, due to constructive interference effects, can give rise to similar phenomena [6] even if the periodic arrays are made of dielectric particles [7–10] . Related to the electromagnetic (EM) field spatial profile, it has been shown that arrays of transparent dielectric nanorods [9] are able to produce huge field enhancements when driven at specific resonant conditions.

The magneto-optical (MO) effect can be used to actively control the behavior of resonant structures or to modulate field enhancements, and, conversely the very same field enhancements can be used to boost the MO signal, which would open new perspectives in device applications, particularly where the resonances have a metallic nature [11, 12]. Also, the use of periodic arrays of micron size MO materials have been used to obtain the magnetic domain structure by means of the study of the MO properties of the diffracted beams [13–16]. The routes to integrated MO systems have been shown recently by different studies, such as those on non-reciprocal optical isolators [17] and sensors [18], or by opening up new perspectives, such as plasmonic interferometry [19, 20], unidirectional plasmonic waveguiding [21], controlled molecular energy transfer [22] and random lasers [23]. A common shortcoming is the relatively weak MO response of usual materials (including ferromagnetics), that needs to be compensated by an enhancement of light–matter interaction, usually from an enhancement of local electric fields. This can be done combining ferromagnetics and noble metals to take advantage of the large local electric field produced by the excitation of surface-plasmons [11, 12, 24]. Another approach is through a periodic molding of the MO structure [25–30]. This magneto-plasmonic enhancement has been demonstrated in multilayer structures [31–34] and nanodiscs or nanoholes arrays [35–39] and is the subject of intense research [40–44].

Most of the previous theoretical approaches to periodic MO structures have been focused on numerical simulations. In this paper we develop an analytical theory to analyze different mechanisms of control and enhancement of the MO response in resonant free-standing MO nanorod arrays. Recent work on arrays of transparent rods [7–9], predicted the existence of high finesse resonances at specific wavelengths and incidence angle of the incoming beam. Recent experiments on free-standing gratings of nanorods [10], made of isotropic dielectric material, reveal the existence of sharp resonances with nearly perfect optical extinction in full agreement with theory [7–9]. Our main goal here is to explore new phenomena arising from the interplay between MO material properties and the geometric optical resonances of the grating.

Based on previous work on the polarizability tensor of anisotropic electrically small particles [45, 46], we first discuss (section 2) the MO response of a single nanowire, under

the assumption of a weak MO response (in comparison to the standard dielectric response). In section 3 we develop an analytical theory of the optical response of subwavelength nanowire gratings made of arbitrary anisotropic materials. When the rods are made of MO dielectric material, we show (section 4) that there is a complex interplay between MO Kerr effects (MOKE) and the geometric resonances of the grating. We will show that, for a given polarization of the incident light, resonant MOKE can be obtained by tuning the incidence angle and grating parameters to operate near the resonance condition for the opposite polarization.

2. Magneto-optical (MO) response of single nanowire

In the presence of a static external magnetic field, the dielectric function of the, otherwise isotropic, nanowire material becomes a tensor of the form [47, 48]

$$\boldsymbol{\epsilon} = \epsilon\,\mathbf{I} + \Delta\boldsymbol{\epsilon} \quad \text{with} \quad \Delta\boldsymbol{\epsilon} = \mathrm{i}Q\epsilon\mathbf{A}, \tag{1}$$

where Q is the MO coefficient, ϵ the isotropic dielectric function in the absence of external magnetic field and $\mathbf{I}$ the unit tensor. $\mathbf{A}$ is the following antisymmetric tensor

$$\mathbf{A} = \begin{pmatrix} 0 & -m_z & m_y \\ m_z & 0 & -m_x \\ -m_y & m_x & 0 \end{pmatrix} \tag{2}$$

written in a direct orthonormal reference frame, with $\hat{\boldsymbol{m}}$ the unit vector in the direction of magnetization.

Let us first define the polarizability of a infinitely long rod made of an anisotropic material with a dielectric tensor $\boldsymbol{\epsilon}$. We consider a cylindrical rod with its axis along the z-axis of subwavelength radius $\mathrm{r_c}$ located in air or vacuum (i.e. in a homogeneous isotropic dielectric medium of permittivity $\epsilon_\mathrm{h} = 1$). We will restrict ourselves to the case in which the external EM fields do not depend on z, i.e. both the electric and the induced dipole in the wire do not depend on z. For simplicity, we will assume incoming monochromatic EM plane waves, $\boldsymbol{E}_0(\boldsymbol{r}) = \boldsymbol{E}_0 \mathrm{e}^{\mathrm{i}\boldsymbol{k}_0\cdot\boldsymbol{r}}$, with frequency ω and wave vector, $\boldsymbol{k}_0 = (K_0\hat{\boldsymbol{x}} - q_0\hat{\boldsymbol{y}})$, perpendicular to the nanowire axis with $|\boldsymbol{k}_0| = k = 2\pi/\lambda = \omega/c$ (the symbol '$\hat{}$' denotes a unit vector).

The induced dipole moment $\boldsymbol{p}_\mathrm{d}$ at a frequency ω can be written as the product of the incident exciting field and the polarizability tensor $\boldsymbol{\alpha}$,

$$\boldsymbol{p}_{\mathrm{d}_j} = \epsilon_0\boldsymbol{\alpha}\boldsymbol{E}_0. \tag{3}$$

The free-space electric polarizability of an anisotropic nanorod can be written as [45]

$$\boldsymbol{\alpha}^{-1} = \boldsymbol{\alpha}_0^{-1} - \mathrm{i}\frac{k^2}{4}\left(\frac{1}{2}\hat{\boldsymbol{x}}\hat{\boldsymbol{x}} + \frac{1}{2}\hat{\boldsymbol{y}}\hat{\boldsymbol{y}} + \hat{\boldsymbol{z}}\hat{\boldsymbol{z}}\right), \tag{4}$$

where $\boldsymbol{\alpha}_0$ is the quasi-static polarizability,

$$\alpha_0^{-1} = \frac{1}{\pi\mathrm{r_c^2}}\left\{\left(\frac{1}{2}\hat{\boldsymbol{x}}\hat{\boldsymbol{x}} + \frac{1}{2}\hat{\boldsymbol{y}}\hat{\boldsymbol{y}}\right)(\boldsymbol{\epsilon}+\mathbf{I}) + \hat{\boldsymbol{z}}\hat{\boldsymbol{z}}\right\}(\boldsymbol{\epsilon}-\mathbf{I})^{-1}. \tag{5}$$

For a MO cylindrical nanorod with $\boldsymbol{\epsilon}$ given by equation (1) we find

$$\boldsymbol{\alpha}_0^{-1} = \boldsymbol{\alpha}_{0\mathrm{I}}^{-1} - \boldsymbol{\Delta}_\mathrm{MO}, \quad \text{with} \quad \boldsymbol{\alpha}_{0\mathrm{I}}^{-1} = \frac{1}{2\pi\mathrm{r_c^2}}\begin{pmatrix} \frac{\epsilon+1}{\epsilon-1} & 0 & 0 \\ 0 & \frac{\epsilon+1}{\epsilon-1} & 0 \\ 0 & 0 & \frac{2}{\epsilon-1} \end{pmatrix}, \tag{6}$$

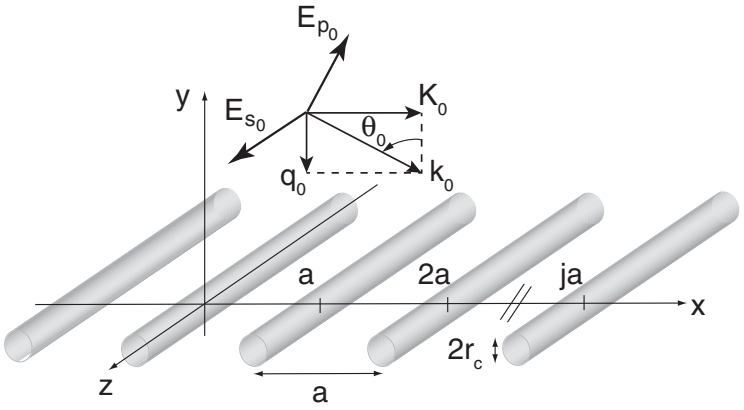

Figure 1. Sketch of the MO nanorod array and of both s and p components of the plane wave incoming at an incidence angle θ_0. The 's' component of the electric field, E_{s_0} is parallel to the nano rod axis ($\hat{\boldsymbol{z}}$) and perpendicular to the plane of incidence ($\hat{\boldsymbol{x}}$, $\hat{\boldsymbol{y}}$) spanned by the surface normal ($\hat{\boldsymbol{y}}$) and the wave vector $\boldsymbol{k}_0$.

where $\boldsymbol{\alpha}_{0\mathrm{I}}$ is the quasi-static polarizability of a cylinder with isotropic dielectric function ϵ and $\boldsymbol{\Delta}_{\mathrm{MO}}$ describes the MO response in the quasi-static limit [46]

$$\boldsymbol{\Delta}_{\mathrm{MO}} = \mathrm{i}\frac{\epsilon Q}{\pi \mathrm{r}_\mathrm{c}^2(\epsilon-1)^2}\mathbf{A} \equiv \mathrm{i}\Delta_{\mathrm{MO}}\mathbf{A}, \tag{7}$$

where we have kept only first-order terms in the MO constant Q.

3. Periodic array of anisotropic nanorods: general results

We consider an infinite set of identical parallel anisotropic nanorods with their axes along the z-axis as sketched in figure 1. The cylinders are located at $\boldsymbol{r}_j = ja\hat{\boldsymbol{x}}$ (with j an integer number). Following previous works on isotropic nanorod gratings [7, 9], we solve the scattering problem using Twersky's [4] multiple-scattering approach.

The field scattered by the nanorod j is given by

$$\boldsymbol{E}_j^{\mathrm{scatt}}(\boldsymbol{r}) = (k^2/\epsilon_0)\mathbf{G}_0(\boldsymbol{r},\boldsymbol{r}_j)\ \boldsymbol{p}_{\mathrm{d}_j} = \{k^2\boldsymbol{p}_{\mathrm{d}_j} + (\boldsymbol{p}_{\mathrm{d}_j}.\boldsymbol{\nabla})\boldsymbol{\nabla}\}g(\boldsymbol{r},\boldsymbol{r}_j),$$

where $\mathbf{G}_0(\boldsymbol{r},\boldsymbol{r}_j)$ and $g(\boldsymbol{r},\boldsymbol{r}_j) = (\mathrm{i}/4)H_0(k|\boldsymbol{r}-\boldsymbol{r}_j|)$ are the 2D free-space Green tensor and scalar function, respectively (H_0 is the Hankel function). The induced dipole, $\boldsymbol{p}_{\mathrm{d}_j}$, is proportional to the actual incident field on the scatterer, $\boldsymbol{p}_{\mathrm{d}_j} = \epsilon_0\boldsymbol{\alpha}\boldsymbol{E}^{\mathrm{in}}(\boldsymbol{r}_j)$. For a periodic array $\boldsymbol{E}^{\mathrm{in}}(\boldsymbol{r}_j) = \boldsymbol{E}^{\mathrm{in}}(\boldsymbol{r}_0)\mathrm{e}^{\mathrm{i}K_0ja}$ and the total field can be written as

$$\boldsymbol{E}(\boldsymbol{r}) = \boldsymbol{E}_0(\boldsymbol{r}) + k^2\left\{\sum_{j=-\infty}^{\infty}\mathrm{e}^{\mathrm{i}K_0ja}\mathbf{G}_0(\boldsymbol{r},\boldsymbol{r}_j)\right\}\boldsymbol{\alpha}\boldsymbol{E}^{\mathrm{in}}(\boldsymbol{r}_0) \equiv \boldsymbol{E}_0(\boldsymbol{r}) + k^2\mathbb{G}^{\pm}(\boldsymbol{r})\boldsymbol{\alpha}\boldsymbol{E}^{\mathrm{in}}(\boldsymbol{r}_0), \tag{8}$$

where the tensor lattice sum $\mathbb{G}^{\pm}(\boldsymbol{r})$ can be written as a sum over all diffracted spectral orders ($m = \ldots, -2, -1, 0, 1, 2, \ldots$) as

$$\mathbb{G}^{\pm}(\boldsymbol{r}) \equiv \left\{\sum_{m=-\infty}^{\infty}\mathrm{e}^{\mathrm{i}K_mx}\mathrm{e}^{\mathrm{i}q_m|y|}\frac{\mathrm{i}}{2aq_m}(\hat{\boldsymbol{p}}_m^{\pm}\hat{\boldsymbol{p}}_m^{\pm} + \hat{\boldsymbol{s}}\hat{\boldsymbol{s}})\right\}, \tag{9}$$

where, following the notations in [49], we have used the unit vectors $\hat{\boldsymbol{s}}$, $\hat{\boldsymbol{p}}_m^+$ and $\hat{\boldsymbol{p}}_m^-$ that define the directions of the electric field in s and p polarizations (for p-polarization, the electric field has two different directions. Here '−' ('+') corresponds to downward transmitted (upward reflected) diffracted waves):

$$q_m \equiv +\sqrt{k^2 - K_m^2}, \qquad K_m \equiv K_0 + \frac{2m\pi}{a}, \tag{10}$$

$$\begin{cases} \hat{\boldsymbol{s}} = \hat{\boldsymbol{x}} \times \hat{\boldsymbol{y}} = \hat{\boldsymbol{z}}, \\ \hat{\boldsymbol{p}}_m^+ = (K_m/k)\hat{\boldsymbol{y}} - (q_m/k)\hat{\boldsymbol{x}} = \sin\theta_m \hat{\boldsymbol{y}} - \cos\theta_m \hat{\boldsymbol{x}}, \\ \hat{\boldsymbol{p}}_m^- = (K_m/k)\hat{\boldsymbol{y}} + (q_m/k)\hat{\boldsymbol{x}} = \sin\theta_m \hat{\boldsymbol{y}} + \cos\theta_m \hat{\boldsymbol{x}}. \end{cases} \tag{11}$$

3.1. Self-consistent field, depolarization tensor and effective polarizability

Each nanorod is excited by the incident plane wave plus the waves scattered from the rest of the grating [4]. The self-consistent incident field, on the $j = 0$ rod, is then given by the solution of

$$\boldsymbol{E}^{\text{in}}(\boldsymbol{r}_0) = \boldsymbol{E}_0(\boldsymbol{r}_0) + k^2 \left\{ \sum_{j\neq 0} \mathrm{e}^{\mathrm{i}K_0 ja} \mathbf{G}_0(\boldsymbol{r}_0, \boldsymbol{r}_j) \right\} \boldsymbol{\alpha} \boldsymbol{E}^{\text{in}}(\boldsymbol{r}_0) \equiv \boldsymbol{E}_0(\boldsymbol{r}) + k^2 \mathbb{G}_b \boldsymbol{\alpha} \boldsymbol{E}^{\text{in}}(\boldsymbol{r}_0), \tag{12}$$

where we introduced the 'depolarization' dyadic $\mathbb{G}_b$,

$$\mathbb{G}_b \equiv \sum_{j\neq 0} \mathrm{e}^{\mathrm{i}K_0 ja} \mathbf{G}_0(\boldsymbol{r}_0, \boldsymbol{r}_j) = \lim_{\boldsymbol{r}\to\boldsymbol{r}_0} \left\{ \mathbb{G}^{\pm}(\boldsymbol{r}) - \mathbf{G}_0(\boldsymbol{r}, \boldsymbol{r}_0) \right\}. \tag{13}$$

(The components of the depolarization dyadic, $\mathbb{G}_b$ (defined by equation (13)) are given in the appendix.)

The self-consistent incident field is then given by

$$\boldsymbol{E}^{\text{in}}(\boldsymbol{r}_0) = \left(1 - k^2 \mathbb{G}_b \boldsymbol{\alpha}\right)^{-1} \boldsymbol{E}_0(\boldsymbol{r}_0), \tag{14}$$

which includes the contribution of both incident (external) and depolarizing (multiple scattering) fields. After substitution of equation (14) in (8) we obtain a simple expression of the total field (outside the nanorods) in terms of the incident plane wave

$$\boldsymbol{E}(\boldsymbol{r}) = \boldsymbol{E}_0(\boldsymbol{r}) + k^2 \mathbb{G}^{\pm}(\boldsymbol{r}) \boldsymbol{\alpha} \left(1 - k^2 \mathbb{G}_b \boldsymbol{\alpha}\right)^{-1} \boldsymbol{E}_0(\boldsymbol{r}_0) \equiv \boldsymbol{E}_0(\boldsymbol{r}) + k^2 \mathbb{G}^{\pm}(\boldsymbol{r}) \boldsymbol{\alpha}_{\text{eff}} \boldsymbol{E}_0(\boldsymbol{r}_0), \tag{15}$$

where $\boldsymbol{\alpha}_{\text{eff}}$ is the effective (dressed) polarizability tensor of each nanorod in the grating,

$$\boldsymbol{\alpha}_{\text{eff}}^{-1} = \boldsymbol{\alpha}_0^{-1} - k^2 \,\text{Re}\left\{\mathbb{G}_b\right\} - \mathrm{i}k^2 \,\text{Im}\left\{\mathbb{G}(0)\right\}. \tag{16}$$

For a subwavelength grating (SWG),

$$\text{Im}\left\{\mathbb{G}(0)\right\} = \frac{1}{2aq_0}\left(\hat{\boldsymbol{s}}\hat{\boldsymbol{s}} + \frac{1}{2}\hat{\boldsymbol{p}}^+\hat{\boldsymbol{p}}^+ + \frac{1}{2}\hat{\boldsymbol{p}}^-\hat{\boldsymbol{p}}^-\right) = \frac{1}{2aq_0}\left\{\hat{\boldsymbol{z}}\hat{\boldsymbol{z}} + \frac{q_0^2}{k^2}\hat{\boldsymbol{x}}\hat{\boldsymbol{x}} + \frac{K_0^2}{k^2}\hat{\boldsymbol{y}}\hat{\boldsymbol{y}}\right\}. \tag{17}$$

3.2. Fresnel transmission and reflection amplitudes in subwavelength gratings

In order to discuss the Fresnel reflection and transmission amplitudes for s and p polarizations, we first write the incident plane wave as

$$\boldsymbol{E}_0(\boldsymbol{r}) = \left(E_{s_0}\hat{\boldsymbol{s}} + E_{p_0}\hat{\boldsymbol{p}}_0^-\right)\mathrm{e}^{\mathrm{i}\boldsymbol{k}_0\boldsymbol{r}} \tag{18}$$

where the unit vectors $\hat{\boldsymbol{s}}$ and $\hat{\boldsymbol{p}}_0^-$ were defined in equation (11). We shall restrict our discussion to SWGs with period $a < \lambda$ below the onset of the first diffracted beam (this takes place at the Rayleigh condition $|K_0 \pm 2\pi/a| = k$). This limits the study to angles of incidence verifying

$$0 \leqslant |\sin\theta_0| \leqslant \frac{2\pi}{ka} - 1 = \frac{\lambda}{a} - 1 \quad \text{or} \quad (K_0 \pm 2\pi/a)^2 > k^2, \tag{19}$$

such that only the zero (specular, $m = 0$) order can propagate in the far field ($|y| \gg \lambda$) input and output regions, being higher-order diffracted beams evanescent and confined in the grating region. From equations (9), (15) and (18) the SWG reflected and transmitted fields are given by

$$\boldsymbol{E}_{\text{refl}}(\boldsymbol{r}) = \left\{\hat{\boldsymbol{s}}\left(r_{ss}E_{s_0} + r_{sp}E_{p_0}\right) + \hat{\boldsymbol{p}}_0^+\left(r_{ps}E_{s_0} + r_{pp}E_{p_0}\right)\right\} \mathrm{e}^{\mathrm{i}K_0 x}\mathrm{e}^{+\mathrm{i}q_0 y}, \tag{20}$$

$$\boldsymbol{E}_{\text{trans}}(\boldsymbol{r}) = \left\{\hat{\boldsymbol{s}}\left(t_{ss}E_{s_0} + t_{sp}E_{p_0}\right) + \hat{\boldsymbol{p}}_0^-\left(t_{ps}E_{s_0} + t_{pp}E_{p_0}\right)\right\} \mathrm{e}^{\mathrm{i}K_0 x}\mathrm{e}^{-\mathrm{i}q_0 y}, \tag{21}$$

where

$$r_{ss} = \frac{\mathrm{i}k^2}{2aq_0}\,\hat{\boldsymbol{s}}\cdot\boldsymbol{\alpha}_{\text{eff}}\hat{\boldsymbol{s}}, \quad r_{ps} = \frac{\mathrm{i}k^2}{2aq_0}\,\hat{\boldsymbol{p}}_0^+\cdot\boldsymbol{\alpha}_{\text{eff}}\hat{\boldsymbol{s}}, \tag{22}$$

$$r_{pp} = \frac{\mathrm{i}k^2}{2aq_0}\,\hat{\boldsymbol{p}}_0^+\cdot\boldsymbol{\alpha}_{\text{eff}}\hat{\boldsymbol{p}}_0^-, \quad r_{sp} = \frac{\mathrm{i}k^2}{2aq_0}\,\hat{\boldsymbol{s}}\cdot\boldsymbol{\alpha}_{\text{eff}}\hat{\boldsymbol{p}}_0^-, \tag{23}$$

$$t_{ss} = 1 + \frac{\mathrm{i}k^2}{2aq_0}\,\hat{\boldsymbol{s}}\cdot\boldsymbol{\alpha}_{\text{eff}}\hat{\boldsymbol{s}}, \quad t_{ps} = \frac{\mathrm{i}k^2}{2aq_0}\,\hat{\boldsymbol{p}}_0^-\cdot\boldsymbol{\alpha}_{\text{eff}}\hat{\boldsymbol{s}}, \tag{24}$$

$$t_{pp} = 1 + \frac{\mathrm{i}k^2}{2aq_0}\,\hat{\boldsymbol{p}}_0^-\cdot\boldsymbol{\alpha}_{\text{eff}}\hat{\boldsymbol{p}}_0^-, \quad t_{sp} = \frac{\mathrm{i}k^2}{2aq_0}\,\hat{\boldsymbol{s}}\cdot\boldsymbol{\alpha}_{\text{eff}}\hat{\boldsymbol{p}}_0^-. \tag{25}$$

In the absence of absorption, equation (16) (with $\boldsymbol{\alpha}_0$ Hermitian) ensures power conservation

$$|r_{ss}|^2 + |r_{ps}|^2 + |t_{ss}|^2 + |t_{ps}|^2 = 1, \tag{26}$$

$$|r_{pp}|^2 + |r_{sp}|^2 + |t_{pp}|^2 + |t_{sp}|^2 = 1. \tag{27}$$

3.3. Dynamic geometrical resonances

Below the onset of the first diffracted beam, all the diffracted modes are evanescent and there is only specular reflection. Near the Rayleigh condition ($|K_0 \pm 2\pi/a| \gtrsim k$) both $\mathrm{Re}(\mathbb{G}_b)_{yy}$ and $\mathrm{Re}(\mathbb{G}_b)_{zz}$ diverge [7, 8] and the lattice sums (see the appendix) can be approximated as

$$\mathrm{Re}(\mathbb{G}_b)_{xx} \approx 0, \tag{28}$$

$$\mathrm{Re}(\mathbb{G}_b)_{yy} \approx \frac{1}{2ak^2}\left(\frac{(K_0 + 2\pi/a)^2}{\sqrt{(K_0 + 2\pi/a)^2 - k^2}} + \frac{(K_0 - 2\pi/a)^2}{\sqrt{(K_0 - 2\pi/a)^2 - k^2}}\right), \tag{29}$$

$$\mathrm{Re}(\mathbb{G}_b)_{zz} \approx \frac{1}{2ak^2}\left(\frac{k^2}{\sqrt{(K_0 + 2\pi/a)^2 - k^2}} + \frac{k^2}{\sqrt{(K_0 - 2\pi/a)^2 - k^2}}\right). \tag{30}$$

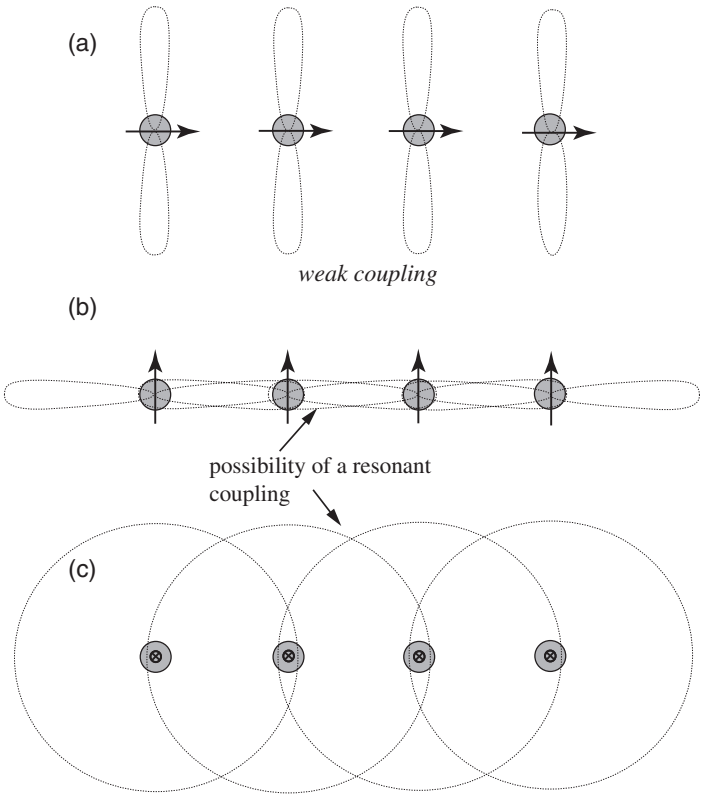

Figure 2. Coupling of dipoles in the grating. The arrows represent the dipole moment induced in the nanorods and the thin lines sketch their respective radiation pattern. (a) The radiation scattered by the dipoles oriented along x is weak in the grating plane and there is no resonant coupling. On the contrary, the coupling between dipoles along y (b) and z (c) can be very strong near the condition of constructive interference, i.e. near the onset of new propagating modes.

The divergences are due to the constructive interference of the scattered fields and are responsible for the so-called geometric resonances of the grating. In the absence of an external magnetic field, for a grating of isotropic rods, the effective polarizability, $\boldsymbol{\alpha}_{\mathrm{eff}} = \boldsymbol{\alpha}_{\mathrm{I}}$, is diagonal with

$$(\alpha_{\mathrm{I}})^{-1}_{xx} \equiv \frac{1}{2\pi r^2}\frac{\epsilon+1}{\epsilon-1} - k^2\,\mathrm{Re}(\mathbb{G}_b)_{xx} - \mathrm{i}\frac{q_0^2}{2aq_0}, \tag{31}$$

$$(\alpha_{\mathrm{I}})^{-1}_{yy} \equiv \frac{1}{2\pi r^2}\frac{\epsilon+1}{\epsilon-1} - k^2\,\mathrm{Re}(\mathbb{G}_b)_{yy} - \mathrm{i}\frac{K_0^2}{2aq_0}, \tag{32}$$

$$(\alpha_{\mathrm{I}})^{-1}_{zz} \equiv \frac{1}{2\pi r^2}\frac{2\epsilon}{\epsilon-1} - k^2\,\mathrm{Re}(\mathbb{G}_b)_{zz} - \mathrm{i}\frac{k^2}{2aq_0}. \tag{33}$$

The coupling of the induced dipoles in the grating, illustrated in figure 2 for non-MO cylindrical nanorods, becomes resonant when the real part of α^{-1}_{Iyy} or α^{-1}_{Izz} vanishes.

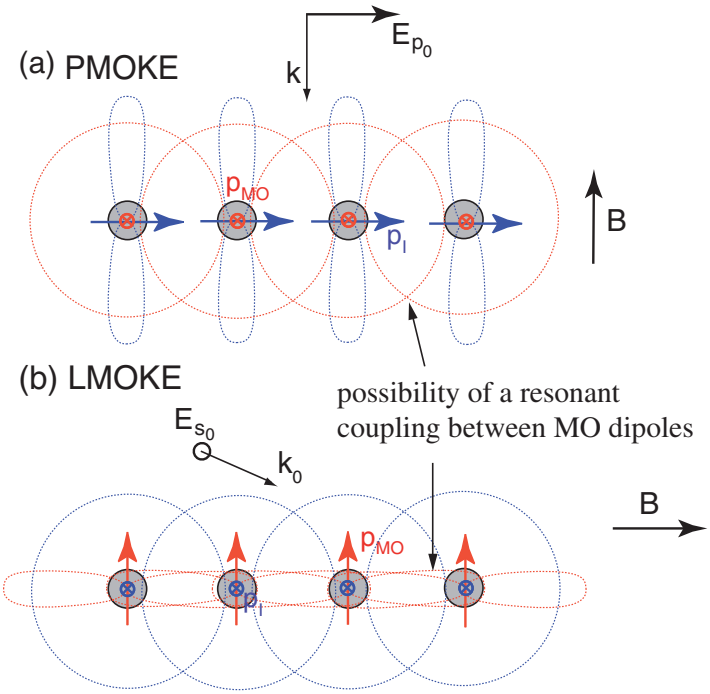

Figure 3. Grating resonances turned on by the MO effect in (a) PMOKE and (b) LMOKE for a normal incidence. In the framework of a first-order study, the dipole moment of a rod is represented by its two components: $\boldsymbol{p}_{\mathrm{I}}$ (blue vector) the isotropic dipole moment (unchanged by the presence of an external magnetic field) and $\boldsymbol{p}_{\mathrm{MO}}$ the MO dipole due to the anisotropic response of the nanorod (see part 2 and [46]).

4. Magneto-optical Kerr effects (MOKE) in subwavelength nanorod gratings

In what follows we will analyze the effect of the geometric lattice resonances on the MO response of the grating. We shall focus the discussion on the lattice resonance effects on the complex Kerr rotation $\theta_{\mathrm{K}} = \theta_{\mathrm{rot}} + \mathrm{i}\varphi_{\mathrm{ell}}$ (where θ_{rot} is the rotation and φ_{ell} is the ellipticity) which can be defined in terms of the ratio between the p and s components of the specular reflected field. Instead of considering an arbitrary external static magnetic field $\boldsymbol{B}$, in order to simplify the discussion, we will consider two different MOKE configurations separately, as illustrated in figure 3. The case $\boldsymbol{B} = B\hat{\boldsymbol{z}}$ (TMOKE) is not studied here since, for $\boldsymbol{k}_0 \perp \hat{\boldsymbol{z}}$, such a magnetic field orientation does not cause an s–p conversion (for a general discussion, see [30]).

In order to illustrate the main physics involved in the different resonant phenomena, we will consider iron garnet materials, which are being used for enhancement of the MO response in various recent applications [42–44]. We will assume a typical iron garnet with approximately real and frequency-independent permittivity $\epsilon \approx 5.5$ (for visible and infrared spectral regions) [50, 51] with off-diagonal elements $Q\epsilon \approx 0.02$ in the visible range [50, 51]. The rod radius $r_{\mathrm{c}} = 50\,\mathrm{nm}$ and the lattice parameter $a = 500\,\mathrm{nm}$ are chosen to have a fixed ratio $r_{\mathrm{c}}/a = 0.1$. Notice that assuming that the permittivity tensor is frequency independent, the results only depend on $\mathrm{r_c}/a$ and a/λ and are scale invariant.

*4.1. Polar MOKE (**B** = Bŷ)*

In the 'polar' configuration (PMOKE), the magnetization vector (the external magnetic field) is oriented perpendicular to the grating plane (and parallel to the plane of incidence) as sketched in figure 3(a). The effective polarizability and Fresnel coefficients can be computed analytically from equation (16) and (7) with $m_z = m_x = 0$ and $m_y = 1$. After some algebra, it is easy to find

$$r_{ss} = \frac{\mathrm{i}k^2}{2q_0 a} \frac{(\alpha_I)_{zz}}{1 - (\alpha_I)_{xx}(\alpha_I)_{zz}\Delta_{\mathrm{MO}}^2} \tag{34}$$

$$r_{sp} = r_{ps} = -\frac{\mathrm{i}k}{2a} \frac{(\alpha_I)_{xx}(\alpha_I)_{zz}\mathrm{i}\Delta_{\mathrm{MO}}}{1 - (\alpha_I)_{xx}(\alpha_I)_{zz}\Delta_{\mathrm{MO}}^2} \tag{35}$$

$$r_{pp} = \frac{\mathrm{i}K_0^2}{2q_0 a}(\alpha_I)_{yy} - \frac{\mathrm{i}q_0^2}{2q_0 a} \frac{(\alpha_I)_{xx}}{1 - (\alpha_I)_{xx}(\alpha_I)_{zz}\Delta_{\mathrm{MO}}^2} \tag{36}$$

Assuming normal incidence, $K_0 = 0$ and $q_0 = k$, as is usually done in PMOKE experimental configurations, there is no resonance for p-polarized waves due to the weak coupling between the scattered field of individual rods (see figure 2(a)). However, the grating presents a sharp resonance for s-polarized incident light for wavelengths close to the onset of diffraction ($a <\approx \lambda$) as illustrated in figure 4(a) where we plot $|r_{ss}|^2$ and $|r_{pp}|^2$ versus a/λ for a SWG. Although $|r_{sp}|^2$ is much smaller than $|r_{ss}|^2$ or $|r_{pp}|^2$, it presents a clear peak at the s resonance as shown in figure 5(a).

4.1.1. s-polarized incident field For s-polarized incident field, apart from a small shift in the resonance frequency or angle (proportional to Δ_{MO}^2), the s resonance is not affected by the external magnetic field. As in the case of isotropic rods, in absence of absorption, the grating present almost perfect reflection at the resonance (i.e. at resonance $r_{ss} \approx 1 - \mathcal{O}(Q^2)$).

For incident s-polarized light the complex Kerr rotation θ_{K} is given by

$$\theta_{\mathrm{K}}^s\big|_{\mathrm{polar}} \equiv -\frac{r_{ps}}{r_{ss}} = \mathrm{i}\frac{q_0}{k}(\alpha_I)_{xx}\Delta_{\mathrm{MO}}. \tag{37}$$

Although both r_{ss} and r_{ps} present a large enhancement at resonance, in this configuration the Kerr angle does not reflect any resonant behavior due to the poor coupling between x dipoles.

4.1.2. p-polarized incident field As we already mentioned, at normal incidence there is no reflection resonance for p-polarized waves (see blue line in figure 4(a)). However, as sketched on figure 3(a), there is a resonant PMOKE effect when the grating is tuned to be resonant for s-polarized waves. At normal incidence the complex Kerr angle, given by

$$\theta_{\mathrm{K}}^p\big|_{\mathrm{polar}} \equiv \frac{r_{sp}}{r_{pp}} = \mathrm{i}(\alpha_I)_{zz}\Delta_{\mathrm{MO}}, \tag{38}$$

is proportional to the effective polarizability $(\alpha_I)_{zz}$. The rotation θ_{rot} is then proportional to $\mathrm{Im}(\alpha_I)_{zz}$ and presents a peak at the s-resonance condition. Analogously, the ellipticity φ_{ell} is proportional to $\mathrm{Re}(\alpha_I)_{zz}$ and changes sign at the resonance (see figure 4(b) and (c)). It is worth noticing that the resonant Kerr rotation has a pure MO origin (coming from r_{sp}, see figure 5(a)) since r_{pp}, in the denominator of equation (38), is a smooth function of a/λ.

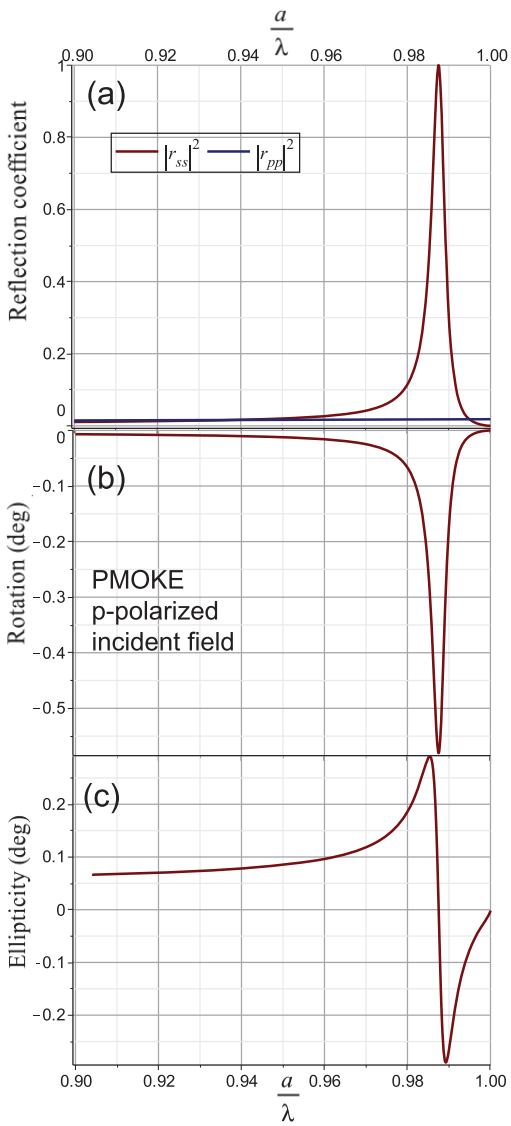

Figure 4. PMOKE at normal incidence: (a) SWG's reflection coefficients, $|r_{ss}|^2$ (red line) and $|r_{pp}|^2$ (blue line) versus a/λ for normal incident. (b) Kerr rotation angle, $\theta^p_{\rm rot}$, and (c) ellipticity, $\varphi^p_{\rm ell}$, of the reflected field versus a/λ for p-polarized incident light. The resonant deep in $\theta^p_{\rm rot}$, as well as the zero ellipticity, coincides with the resonant condition for s-polarized waves. (System parameters: $\epsilon = 5.5$, $Q\epsilon = 0.02$, $\mathrm{r_c}/a = 0.1$ and $\theta_0 = 0$, see text.)

Just at the s resonance, in absence of absorption, the real part of $(\alpha_I)_{zz}$ is zero and

$$\theta^p_{\rm rot}\big|_{\rm polar} = -Q\frac{\epsilon}{(\epsilon-1)^2}\frac{a\lambda}{\pi^2 \mathrm{r_c^2}}, \tag{39}$$

$$\varphi^p_{\rm ell}\big|_{\rm polar} = 0. \tag{40}$$

Since $\mathrm{r_c} \ll \lambda$, the reflected light, at resonance, is linearly polarized with a large Kerr rotation. For metallic rods, however, the real part of ϵ is typically negative and there are no s resonances [7].

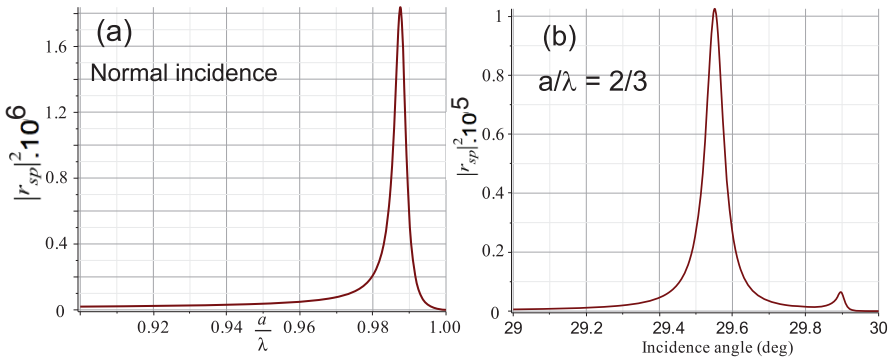

Figure 5. Non-diagonal reflectance, $|r_{sp}|^2$ (accounting for polarization conversion), (a) versus a/λ for normal incidence and (b) versus the angle of incidence θ_0 for fixed $a/\lambda = 2/3$. At normal incidence $|r_{sp}|^2$ presents a single maximum (just at the s-resonance wavelength of the SWG). In contrast, at fixed wavelength, the peaks at two different angles correspond to the MO coupling to both s and p grating resonances. (System parameters: $\epsilon = 5.5$, $Q\epsilon = 0.02$, $r_c/a = 0.1$.)

This configuration should then be useful for dielectric MO materials but not very appropriate for metallic nanowires.

4.2. Longitudinal MOKE ($\boldsymbol{B} = B\hat{\boldsymbol{x}}$)

Let us assume that the external magnetic field is in the plane of incidence but oriented parallel to the grating plane (and perpendicular to the nanorods) with $m_z = m_y = 0$ and $m_x = 1$. For this magnetic field configuration, known as longitudinal MOKE (LMOKE), we have

$$r_{ss} = \frac{\mathrm{i}k^2}{2q_0 a} \frac{(\alpha_I)_{zz}}{1 - (\alpha_I)_{yy}(\alpha_I)_{zz}\Delta_{\mathrm{MO}}^2}, \tag{41}$$

$$r_{sp} = r_{ps} = -\frac{\mathrm{i}kK_0}{2aq_0} \frac{(\alpha_I)_{yy}(\alpha_I)_{zz}\mathrm{i}\Delta_{\mathrm{MO}}}{1 - (\alpha_I)_{yy}(\alpha_I)_{zz}\Delta_{\mathrm{MO}}^2}, \tag{42}$$

$$r_{pp} = -\frac{\mathrm{i}q_0^2}{2q_0 a}(\alpha_I)_{xx} + \frac{\mathrm{i}K_0^2}{2q_0 a} \frac{(\alpha_I)_{yy}}{1 - (\alpha_I)_{yy}(\alpha_I)_{zz}\Delta_{\mathrm{MO}}^2}. \tag{43}$$

At normal incidence $r_{sp} = 0$ and there is no LMOKE effect. However, at fixed wavelength ($a < \lambda < 2a$), the SWG's reflection coefficients show well-defined peaks as a function of the angle of incidence (again, near the onset of diffracted beams) as shown in figure 6(a) where we plot $|r_{ss}|^2$ and $|r_{pp}|^2$ versus θ_0 for $a/\lambda = 2/3$. $|r_{sp}|^2$ (see figure 5(b)) exhibits two resonant peaks associated to both s and p resonances, the peak at the p resonance being almost one order of magnitude larger than the corresponding s resonance (the latter is of the same order than the one discussed for normal incidence as shown in figure 5(a); notice the different scales in figures 5(a) and (b)).

4.2.1. s-polarized incident field For s-polarized incident light, the complex Kerr angle is given by

$$\theta_{\mathrm{K}}^s\big|_{\mathrm{long}} \equiv -\frac{r_{ps}}{r_{ss}} = \mathrm{i}\frac{K_0}{k}(\alpha_I)_{yy}\Delta_{\mathrm{MO}} \tag{44}$$

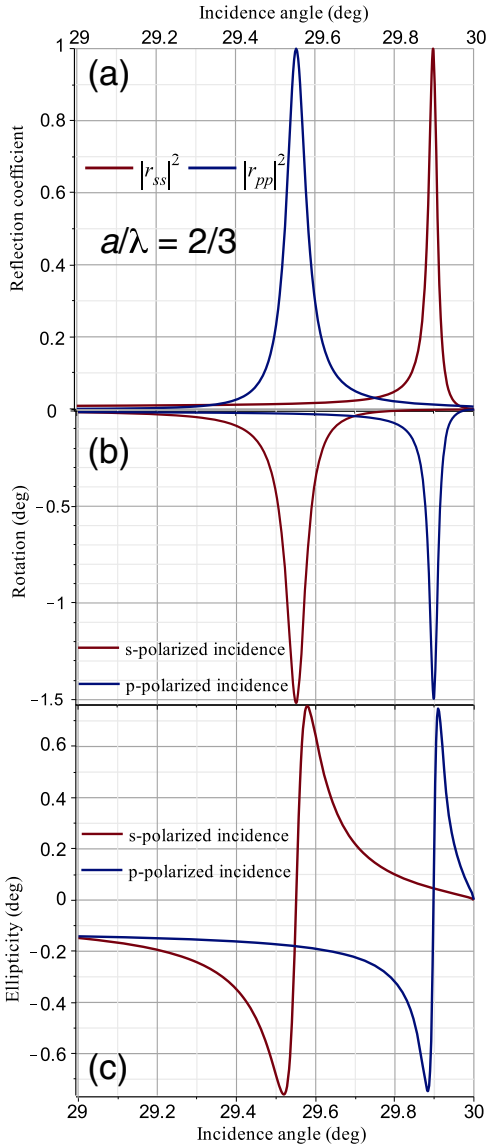

Figure 6. LMOKE at fixed wavelength: (a) SWG's reflection coefficients, $|r_{ss}|^2$ (red line) and $|r_{pp}|^2$ (blue line) versus the angle of incidence θ_0. (b) Kerr rotation angles versus θ_0 for p-polarized ($\theta^p_{\rm rot}$, blue line) and s-polarized ($\theta^s_{\rm rot}$, red line) incident light. (c) Ellipticity of the reflected field, $\varphi^p_{\rm ell}$ (blue line), and $\varphi^s_{\rm ell}$ (red line) versus $a\lambda$. Notice that, for a given polarization of the incident light, resonant LMOKE rotation is obtained at the resonance condition for the opposite polarization. (System parameters: $\epsilon = 5.5$, $Q\epsilon = 0.02$, $\mathrm{r_c}/a = 0.1$ and $a/\lambda = 2/3$, see the text.)

which is now proportional to $(\alpha_I)_{yy}$ and, as a consequence, rotation and ellipticity for s incidence present a resonant dip at $\theta_0 = \theta_{p-\rm res}$ (see red line in figure 6(b)), the angle at which the reflectance presents a maximum for p-polarized waves (see blue line in figure 6(a)). At the resonant condition, $\theta_0 = \theta_{p-\rm res}$, we have

$$\theta^s_{\rm rot}\big|_{\rm long} = -Q\frac{\epsilon}{(\epsilon-1)^2}\frac{a\lambda}{\pi^2 \mathrm{r_c^2}\tan\theta_{p-\rm res}} \tag{45}$$

$$\varphi^{s}_{\rm ell}\big|_{\rm long} = 0. \tag{46}$$

Again, we obtain a resonant enhancement of the Kerr rotation due to the lattice geometrical resonances as described in figure 3(b).

4.2.2. p-polarized incident field For $K_0 \neq 0$, r_{pp} can present the well-known zero reflection condition at the Brewster's angle. This would lead to an 'optically' enhanced Kerr angle which is not actually related to an enhanced MO response. Near the diffraction onset, and far from the Brewster's angle, we can neglect the contribution of $(\alpha_I)_{xx}$ in equation (43) obtaining

$$\theta^{p}_{K}\big|_{\rm long} \equiv -\frac{r_{sp}}{r_{pp}} \approx {\rm i}\frac{k}{K_0}(\alpha_I)_{zz}\Delta_{\rm MO}, \tag{47}$$

i.e. near the onset of diffraction, the Kerr angle is proportional to $(\alpha_I)_{zz}$. We then find that rotation and ellipticity for p incidence present a resonant dip at $\theta_0 = \theta_{s-{\rm res}}$ (see blue line in figure 6(b)), the angle at which the reflectance presents a maximum for s-polarized waves (see red line in figure 6(a)). At the s resonance,

$$\theta^{p}_{\rm rot}\big|_{\rm long} = -Q\frac{\epsilon}{(\epsilon-1)^2}\frac{a\lambda\tan\theta_{s-{\rm res}}}{\pi^2 {\rm r}_{\rm c}^2}, \tag{48}$$

$$\varphi^{p}_{\rm ell}\big|_{\rm long} = 0. \tag{49}$$

5. Conclusions

We have presented an analytical theory of the optical response of subwavelength nanowire gratings made of anisotropic materials. We have shown that when the rods are made of MO dielectrics there is a complex interplay between the geometric resonances of the grating and the MOKE response. As a general conclusion, for a given polarization of the incident light, resonant MOKE can be obtained by tuning the incidence angle and grating parameters to operate near the resonant reflectance condition for the opposite polarization, i.e. for s incidence the grating should be at the resonance condition for p polarization and viceversa.

It is worthwhile to mention that in our theoretical description we assumed a perfect (infinite) periodic grating with infinitely long nanowires as well as plane wave illumination. In practice, for actual laser beams, we expect to see important differences if the beam waist is smaller than a few wavelengths or larger than the grating size. In the case of very small nano rods (i.e. nanorod lengths much smaller than the wavelength), the system will be similar to a one-dimensional chain of parallel ellipsoids [21]. Our discussion did not consider any possible resonant (antenna-like) effects associated with intermediate nanowire length, which could be a very interesting topic in itself.

Our results may be important to understand and optimize MOKE structures and devices based on resonant SWGs. Extension of the analysis presented here will allow one to understand further unexplored resonant effects in diffracted beams.

Acknowledgments

RC acknowledges the DIPC at San Sebastian (Spain) where part of this work was done. This work was supported by Ikerbasque Visiting Fellowship (JJS), EU Project Nanomagma NMP3-SL-2008-214107, by LABEX WIFI (Laboratory of Excellence within the French Program

'Investments for the Future') under references ANR-10-LABX-24 and ANR-10-IDEX-0001-02 PSL*, by the Spanish Ministerio de Ciencia e Innovación through CSD2007-00046 (NanoLight.es); CSD2008-00023 (Funcoat); FIS2009-13430 ; MAT2011-29194-C02-01; FIS2012-3611 and by the Comunidad de Madrid P2009/TIC-1476.

Appendix

The sums involved in the calculation of the depolarization dyadic $\mathbb{G}_b$ in equation (13) are, in this form, dramatically slowly convergent. Fortunately, they are found to be equal to (see, after correction of a minor sign error, equations (7), (20), (21) in [7]):

$$\begin{cases} (\mathbb{G}_b)_{xx} = \dfrac{1}{2ak^2}\displaystyle\sum_{m=1}^{\infty}\left(\mathrm{i}q_m + \mathrm{i}q_{-m} + 2k_m - \dfrac{k^2}{k_m}\right) + \dfrac{q_0^2}{k^2}\dfrac{\mathrm{i}}{2aq_0} + \dfrac{1}{4\pi}\left[\ln\left(\dfrac{ka}{4\pi}\right) + \gamma_\mathrm{E} - \dfrac{1}{2}\right] \\ \qquad\qquad + \dfrac{\pi}{6a^2k^2} - \dfrac{\mathrm{i}}{8}, \\ (\mathbb{G}_b)_{yy} = \dfrac{1}{2ak^2}\displaystyle\sum_{m=1}^{\infty}\left(\dfrac{\mathrm{i}(k_m - K_0)^2}{q_m} + \dfrac{\mathrm{i}(k_m + K_0)^2}{q_{-m}} - 2k_m - \dfrac{k^2}{k_m}\right) + \dfrac{K_0^2}{k^2}\dfrac{\mathrm{i}}{2aq_0} \\ \qquad\qquad + \dfrac{1}{4\pi}\left[\ln\left(\dfrac{ka}{4\pi}\right) + \gamma_\mathrm{E} + \dfrac{1}{2}\right] - \dfrac{\pi}{6a^2k^2} - \dfrac{\mathrm{i}}{8}, \\ (\mathbb{G}_b)_{zz} = \dfrac{1}{2a}\displaystyle\sum_{m=1}^{\infty}\left(\dfrac{\mathrm{i}}{q_m} + \dfrac{\mathrm{i}}{q_{-m}} - \dfrac{2}{k_m}\right) + \mathrm{i}\left(\dfrac{1}{2aq_0} - \dfrac{1}{4}\right) + \dfrac{1}{2\pi}\left[\ln\left(\dfrac{ka}{4\pi}\right) + \gamma_\mathrm{E}\right], \end{cases} \tag{A.1}$$

where $k_m = 2\pi m/a$, $q_m = \sqrt{k^2 - (K_0 + k_m)^2}$, γ_E is the Euler constant. These expressions can be easily computed.

References

[1] Wood R W 1902 *Proc. R. Soc. Lond.* A **18** 269
[2] Fano U 1941 *J. Opt. Soc. Am.* **31** 213
[3] Rayleigh L 1907 *Proc. R. Soc. Lond.* A **79** 399
[4] Twersky V 1952 *J. Appl. Phys.* **23** 1099
[5] Ebbesen T W, Lezec H J, Ghaemi H F, Thio T and Wolf P A 1998 *Nature* **391** 667
[6] García de Abajo F J, Gómez-Medina R and Sáenz J J 2005 *Phys. Rev.* E **72** 016608
[7] Gómez-Medina R, Laroche M and Sáenz J J 2006 *Opt. Express* **14** 3730
[8] Laroche M, Albaladejo S, Gómez-Medina R and Sáenz J J 2006 *Phys. Rev.* B **74** 245422
[9] Laroche M, Albaladejo S, Carminati R and Sáenz J J 2007 *Opt. Lett.* **32** 2762
[10] Ghenuche P, Vincent G, Laroche M, Bardou N, Haïdar R, Pelouard J-L and Collin S 2012 *Phys. Rev. Lett.* **109** 143903
[11] Armelles G, Cebollada A, García-Martín A and González M U 2013 *Adv. Opt. Mater.* **1** 10
[12] Armelles G, Cebollada A, García-Martín A, García-Martín J M, González M U, González-Díaz J B, Ferreiro-Vila E and Torrado J F 2009 *J. Opt. A: Pure Appl. Opt.* **11** 114023
[13] García-Mochales P, Costa-Krämer J L, Armelles G, Briones F, Jaque D, Martín J I and Vicent J L 2002 *Appl. Phys. Lett.* **81** 3206
[14] Grimsditch M P and Vavassori P 2004 *J. Phys.: Condens. Matter.* **16** R275

[15] Bengoeechea A, Armelles G, Costa-Krämer J L and Anguita J 2006 *Phys. Rev.* B **73** 205402
[16] Verduci T, Rufo C, Berger A, Metlushko V, Ilic B and Vavassori P 2011 *Appl. Phys. Lett.* **99** 092501
[17] Espinola R L, Izuhara T, Tsai M-C, Osgood R M and Dötsch H 2004 *Opt. Lett.* **29** 941
[18] Regatos D, Fariña D, Calle A, Cebollada A, Sepúlveda B, Armelles G and Lechuga L M 2010 *J. Appl. Phys.* **108** 054502
[19] Martín-Becerra D, González-Díaz J B, Temnov V V, Cebollada A, Armelles G, Thomay T, Leitenstorfer A, Bratschitsch R, García-Martín A and González M U 2010 *Appl. Phys. Lett.* **97** 183114
[20] Temnov V V, Armelles G, Woggon U, Guzatov D, Cebollada A, García-Martín A, García-Martín J M, Thomay T, Leitenstorfer A and R Bratschitsch R R 2010 *Nature Photon.* **4** 107
[21] Hadad Y and Steinberg B Z 2010 *Phys. Rev. Lett.* **105** 233904
[22] Vincent R and Carminati R 2011 *Phys. Rev.* B **83** 165426
[23] Pinheiro F A 2008 *Phys. Rev.* A **78** 023812
[24] Safarov V I, Kosobukin V A, Hermann C, Lampel G, Peretti J and Marlière C 1994 *Phys. Rev. Lett.* **73** 3584
[25] Inoue M, Arai K, Fujii T and Abe M 1998 *J. Appl. Phys.* **83** 6768
[26] Kato H, Matsushita T, Takayama A, Egawa M, Nishimura K and Inoue M 2003 *J. Appl. Phys.* **93** 3906
[27] Wang Z and Fan S 2005 *Opt. Lett.* **30** 1989
[28] Zharov A and Kurin V 2007 *J. Appl. Phys.* **102** 123514
[29] Smigaj W, Romero-Vivas J, Gralak B, Magdenko L, Dagens B and Vanwolleghem M 2010 *Opt. Lett.* **35** 568
[30] Pimenov I and Kurin V 2012 *J. Opt. Soc. Am.* B **29** 1815
[31] Hermann C, Kosobukin V A, Lampel G, Peretti J, Safarov V I and Bertrand P 2001 *Phys. Rev.* B **64** 235422
[32] González-Díaz J B, García-Martín A, Armelles G, García-Martín J M, Clavero C, Cebollada A, Lucaszew R A, Skuza J R, Kumah D P and Clarke R 2007 *Phys. Rev.* B **76** 153402
[33] Ferreiro-Vila E, González-Díaz J B, Fermento R, González M U, García-Martín A, García-Martín J M, Cebollada A, Armelles G, Meneses-Rodríguez D and Muñoz-Sandoval E 2009 *Phys. Rev.* B **80** 125132
[34] Caballero B, García-Martín A and Cuevas J C 2012 *Phys. Rev.* B **85** 245103
[35] Torrado J F, González-Díaz J B, González M U, García-Martín A and Armelles G 2010 *Opt. Express* **18** 15635
[36] Papaioannou E T, Kapaklis V, Patoka P, García-Martín A, Ferreiro-Vila E and Ctistis G 2010 *Phys. Rev.* B **81** 054424
[37] Melander E *et al* 2012 *Appl. Phys. Lett.* **110** 063107
[38] Alcaraz de la Osa R, Saiz J M, Moreno F, Vavassori P and Berger A 2012 *Phys. Rev.* B **85** 064414
[39] Banthí J C, Meneses-Rodríguez D, García F, González M U, García-Martín A, Cebollada A and Armelles G 2012 *Adv. Mater.* **24** 36
[40] Belotelov V I, Akimov I A, Pohl M, Kotov V A, Kasture S, Vengurlekar A S, Gopal A V, Yakovlev D R, Zvezdin A K and Bayer M 2011 *Nature Nanotechnol.* **6** 370–6
[41] Fevrier M, Gogol P, Aassime A, Megy R, Delacour C, Chelnokov A, Apuzzo A, Blaize S, Lourtioz J M and Dagens B 2012 *Nano Lett.* **12** 1032–7
[42] Chin J Y, Steinle T, Wehlus T, Dregely D, Weiss T, Belotelov V I, Stritzker B and Giessen H 2013 *Nature Commun.* **4** 1599
[43] Belotelov V I *et al* 2013 *Nature Commun.* **4** 2128
[44] Baryshev A V, Uchida H and Inoue M 2013 *J. Opt. Soc. Am.* B **30** 2371
[45] Albaladejo S, Gómez-Medina R, Froufe-Pérez L S, Marinchio H, Carminati R, Armelles G, Torrado J, García-Martín A and Sáenz J J 2010 *Opt. Express* **18** 3556
[46] Marinchio H, Sáenz J J and Carminati R 2012 *Phys. Rev.* B **85** 245425
[47] Hunt R P 1967 *J. Appl. Phys.* **38** 1652
[48] Zak J, Moog E R, Liu C and Bader S D 1990 *J. Magn. Magn. Mater.* **89** 107
[49] Sipe J E 1987 *J. Opt. Soc. Am.* B **4** 481
[50] Hansteen F, Helseth L E, Johansen T H, Hunderi O, Kirilyuk A and Rasing Th 2004 *Thin Solid Films* **455–456** 429
[51] Wurtz G A, Hendren W, Pollard R, Atkinson R, Le Guyader L, Kirilyuk A, Rasing Th, Smolyaninov I I and Zayats A V 2008 *New J. Phys.* **10** 105012